

## An analysis of the mechanism of Kerr effect enhancement in Mn/Dy/Bi

S. G. Ovchinnikov, L. V. Burkova, V. A. Seredkin, and V. Yu. Yakovchuk

*L. V. Kirenskiĭ Institute of Physics, Siberian Branch of the Russian Academy of Sciences, 660036 Krasnoyarsk, Russia*

(Submitted June 2, 1998)

Fiz. Tverd. Tela (St. Petersburg) **41**, 91–97 (January 1999)

A study is reported of the structural, magnetic, and magneto-optic properties of Mn/Dy/Bi films obtained by multilayer technology. The maximum Kerr rotation angle in such films is shown to be  $\theta_k = 2.25^\circ$ . Possible reasons for such a large Kerr effect enhancement are considered, namely, an increase in the  $6p-3d$  transition probability caused by symmetry distortion, polarization of the Bi $6p$  band, and a change in the density of states near the Fermi level. The latter reason has been analyzed by simulating the electronic structure of Mn/Dy/Bi through superposition of Dy levels on the MnBi band structure. This approach has revealed possible additional transitions which may be induced by the presence of a Dy buffer and could contribute to the Kerr magneto-optic effect. © 1999 American Institute of Physics. [S1063-7834(99)02001-8]

MnBi polycrystalline films were one of the first materials<sup>1</sup> in which a large room-temperature Kerr effect ( $\theta_k = 0.7^\circ$ ) was observed<sup>2</sup>. Mn/Dy/Bi films, obtained presently by multilayer technology, exhibit, besides a reduction of mean crystallite size to 15 nm and an increased perpendicular anisotropy, a rotation angle of  $2.25^\circ$  (Ref. 3), which is of considerable interest from both scientific and applications standpoints. Experiment shows that incorporation into the bulk of the film of such impurities as Ti,<sup>4</sup> Zn, Te,<sup>5</sup> Sb,<sup>6</sup> V, Cr, Cu, Ni,<sup>7</sup> Ag, Au, In, Pt,<sup>8</sup> as well as of Dy,<sup>9</sup> results in degradation of the magneto-optic (MO) properties. While Al doping enhances the Kerr effect<sup>8,10</sup> up to  $2^\circ$ , it reduces at the same time the perpendicular anisotropy by one half. Using Sm, Ce, and Pr<sup>11</sup> as dopants permits one to obtain rotation angles of 2 to  $2.5^\circ$ , but the hysteresis loop rectangulativity ratio becomes less than unity.

Self-consistent calculations of the MnBi spin-polarized band structure, in which spin-orbit interaction was considered as a perturbation, showed that the main contribution to the MO effect should come from Bi $6p\downarrow \rightarrow$  Mn $3d\downarrow$  transitions.<sup>12</sup> Relativistic electronic-structure calculations made in the local density-functional augmented spherical-wave (LDA-ASW) approximation yield a spectral response of the Kerr effect in MnBi which agrees well with experiment.<sup>13,14</sup> Using this approach in an analysis of the microscopic nature of the Kerr effect in MnBi permitted one to relate its large values to a combination of the fairly large magnetic moment on Mn, a strong spin-orbit Bi coupling, which is believed to be ten times larger than that in  $3d$  metals,<sup>15</sup> and a strong hybridization between the Mn $d$  band and Bi $p$  states<sup>14</sup>. A theoretic consideration<sup>13,16</sup> of the effect of impurities on the Kerr effect shows that their presence gives rise to a change in Mn magnetization and Bi spin-orbit coupling<sup>16</sup> and a redistribution of the density of states near the Fermi level and affects the hybridization,<sup>13,16</sup> while the magnitude of the MO effect depends to a considerable extent on the position of the impurity atoms in the MnBi cell (Ref. 13). The latter conclu-

sion is consistent with cluster-model calculations<sup>17</sup>. An analysis of experimental data gives one grounds to assume that the relative significance of the above contributions to the Kerr effect is determined by the characteristics of the dopant.<sup>8,11</sup>

This work reports an investigation of the structural, magnetic, and magneto-optic properties of Mn/Dy/Bi films and analyzes the mechanism responsible for the considerable enhancement of the Kerr effect ( $\theta_k = 2.25^\circ$ ) observed in these films.

### 1. SAMPLES AND EXPERIMENTAL METHOD

Mn/Dy/Bi films were prepared by successive deposition of alternating Bi, Dy, Mn, Dy etc. layers on glass substrates at room temperature in a vacuum of  $3 \times 10^{-6}$  Torr.<sup>18</sup> Immediately after the deposition, the samples were annealed in a vacuum of  $5 \times 10^{-6}$  Torr at a temperature of 250–270 °C. The anneal times were chosen 60, 30, 15, and 7 min, depending on the thickness and number of layers.<sup>19</sup> The thicknesses of the Bi and Mn layers were chosen so as to satisfy the 1:1 atomic ratio, and varied within the 12.5–100-nm interval for Bi, and from 4 to 39 nm for Mn. The Dy layer thickness was varied from 3 to 40 nm.

The structural properties of the films were studied by transmission electron microscopy. The chemical composition and thickness of the samples were determined by spectral fluorescence analysis. Auger spectra permitted measuring the distribution of components through the thickness. Chemical bonding was derived from X-ray photoelectron (XPS) spectra. The saturation magnetization ( $M_s$ ) and the perpendicular anisotropy constant ( $K_u$ ) were measured with a torsion magnetometer. The polar Kerr-effect rotation ( $\theta_k$ ) and its spectral response were obtained from the side of the substrate at room temperature on a magneto-optic setup in fields of up to 16 kOe. The coercive force ( $H_c$ ) was extracted from Kerr hysteresis loops.

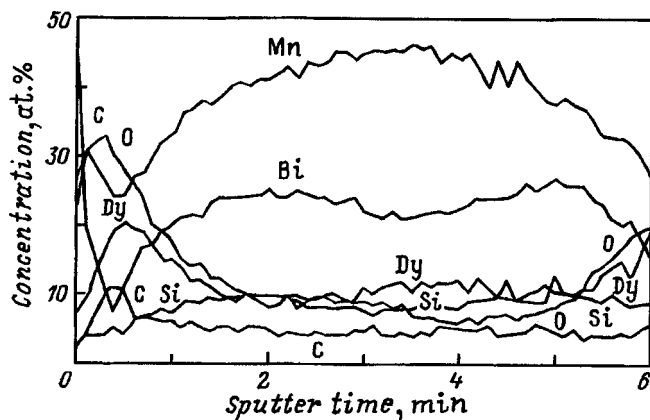


FIG. 1. Auger depth profile of a Mn/Dy/Bi film.

## 2. EXPERIMENTAL RESULTS

The characteristics of Mn/Dy/Bi films optimized in thickness and number of layers in the starting condition were as follows: average crystallite size 15 nm,  $H_c = 6$  kOe,  $K_u = 1 \times 10^7$  erg/cm<sup>3</sup>, and  $\theta_k = 2.25^\circ$  for  $\lambda = 633$  nm. Before annealing, these films consisted of alternating Bi, Dy, and Mn layers of thickness 49.5, 5, and 17 nm, respectively, with the total number of layers being seven. They were annealed at 270 °C for 30 min.

A comparative analysis of the crystalline structure of these films and of MnBi films fabricated by standard technology<sup>20</sup> shows that the considerable decrease in crystallite size in the former is due to introducing Dy as a buffer. After annealing, MnBi films contain a lot of large crystallites 250–400 nm in size, with some of them measuring 1000–3000 nm. The average size of crystallites in structurally optimum Mn/Dy/Bi films decreases after annealing from 300 to 15 nm, i.e., by nearly two orders of magnitude compared to MnBi. The electron diffraction patterns of Mn/Dy/Bi films obtained before annealing show Bi, Dy, and Mn to be polycrystalline, with the average size of Bi and Mn crystallites about 300 nm, and that of Dy crystallites, an order of magnitude smaller. After the annealing, one observes besides the newly formed MnBi phase a small volume fraction of Mn and Bi as a free phase. Annealing reduces considerably the volume fraction of pure Dy, which may be due to its incorporation into the MnBi lattice. Formation of Dy compounds with oxygen and/or Mn oxide is also possible, which finds support in the presence of a DyMnO<sub>3</sub> reflection in the electron diffraction patterns and XPS spectra. These spectra reveal the presence of Bi and Mn in metallic state, and Dy, both in metallic and oxidized states.

Figure 1 shows an Auger depth profile of a Mn/Dy/Bi film showing that the distribution of each component is sufficiently uniform throughout the volume of the film. The enhanced content of oxygen and dysprosium in the near-surface and near-substrate regions can be attributed to a tendency characteristic of RE elements to migrate to the film surface and become oxidized there.<sup>21</sup>

A detailed analysis of the structural features of Mn/Dy/Bi compared with MnBi films permits a conclusion that multilayer technology favors formation of a fine-grained

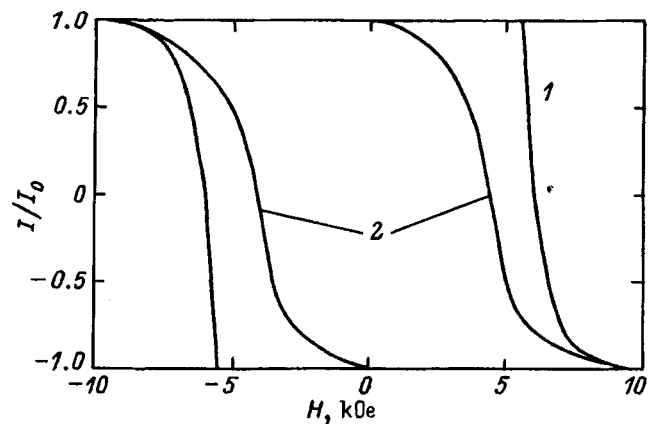


FIG. 2. Hysteresis loops of (1) Mn/Dy/Bi and (2) MnBi films.

crystalline structure.<sup>3</sup> Doping with Dy by sandwiching the corresponding buffer layer favors a more uniform distribution of Dy atoms in the bulk of the film in the course of annealing and their incorporation in the crystal lattice, and there are grounds to assume that they preferably occupy intermediate positions in the MnBi cell and/or substitute for Bi,<sup>11</sup> but not for Mn (Ref. 4). One cannot exclude a possibility that a small fraction of Dy segregates to form a separate phase rather than entering a solid solution. If the content of the Dy dopant is small, this phase will apparently become distributed over MnBi grain boundaries, and for large contents pure Dy inclusions will appear.

Figure 2 presents a room-temperature hysteresis loop of a Mn/Dy/Bi film with optimum parameters. A comparison with the loop of a MnBi film obtained by us by standard technology indicates that a Dy buffer improves considerably the hysteresis-loop rectangularity ratio, which for all the Mn/Dy/Bi films is unity. Table I lists the magnetic and magneto-optic parameters of Mn/Dy/Bi films having different thicknesses and number of layers before anneal. Also presented are the parameters of MnBiDy and MnBi films fabricated by us using standard technology, and the relevant data available from the literature. As seen from Table I, the Kerr rotation angle for all Mn/Dy/Bi films is larger than that quoted for MnBi. The largest value  $\theta_k$  was measured in the above-mentioned films with optimum parameters. The MO rotation in films prepared by us by conventional Dy doping at the equivalent percentage level is smaller, 0.35° (Table I). Figure 3 shows the spectral response of  $\theta_k$  for Mn/Dy/Bi films, which is seen to peak around  $\lambda = 633$  nm. This maximum is slightly shifted toward shorter wavelengths compared to the corresponding relation for MnBi films also displayed in the figure.

## 3. DISCUSSION OF RESULTS

Note the large Kerr rotation angle in Mn/Dy/Bi films, whose maximum value exceeds by 1.5 times the value obtained by us in MnBi films (Table I). As already mentioned, Kerr rotation depends on the spin-orbit coupling, magnetization, and density of states.<sup>15</sup> Our measurements showed that the magnetization of Mn/Dy/Bi films is about 30% less than that of our MnBi films. This may be due to a large extent to

TABLE I. Magnetic and magneto-optic properties of Mn/Dy/Bi, MnBiDy, and MnBi films.

Composition	Thickness			Total number of layers	Anneal time, min	$H_c$ , kOe	$M_s$ , G	$K_u \cdot 10^{-7}$ , erg/cm <sup>3</sup>	$\theta_k$ , deg
	Bi, nm	Mn, nm	Dy, nm						
Mn/Dy/Bi	49.5	17	5	3	30	2	485	1	1.5
Mn/Dy/Bi	49.5	17	20	3	60	5	—	—	1.4
Mn/Dy/Bi	50	18	4	7	30	1.6	520	1.2	1.9
Mn/Dy/Bi	104	39	5	3	60	4.7	320	0.7	1.0
Mn/Dy/Bi	49.5	17	5	7	30	6	330	1.4	2.25
MnBiDy		148			30	8			0.35
MnBi		148			60	3.5	400	1.4	1.3
MnBi [13]		148			300	0.8	620	20	0.7

the formation of a fine-grained crystalline structure.<sup>17</sup> Calculations suggest that incorporation of an impurity, e.g. Al, in MnBi results in a decrease in the spin-orbit coupling because of the impurity and Bi states becoming hybridized.<sup>16</sup> It thus appears hardly likely that the former two reasons could contribute to the increase of  $\theta_k$ , and the explanation should be sought rather in a change of the electronic structure induced by the presence of a Dy buffer.

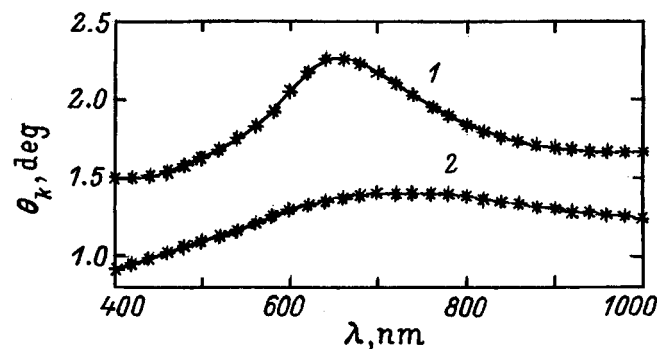
To picture more clearly the mechanism of Kerr effect enhancement, consider the MnBi band structure,<sup>12</sup> whose calculated density of states is shown in Fig. 4a–4c. We readily see that the Bi6p $\downarrow$   $\rightarrow$  Mn3d $\downarrow$  optic transitions with energies of 1.5–2 eV have the highest probability. Quantitative calculations support this conclusion.<sup>13,14</sup> The calculated spectral response passes through a maximum at 1.8 eV, which agrees with both our (Fig. 3) and other available experimental data.

Phenomenological consideration identifies Kerr rotation with the off-diagonal term of the optical conductivity tensor<sup>15</sup>

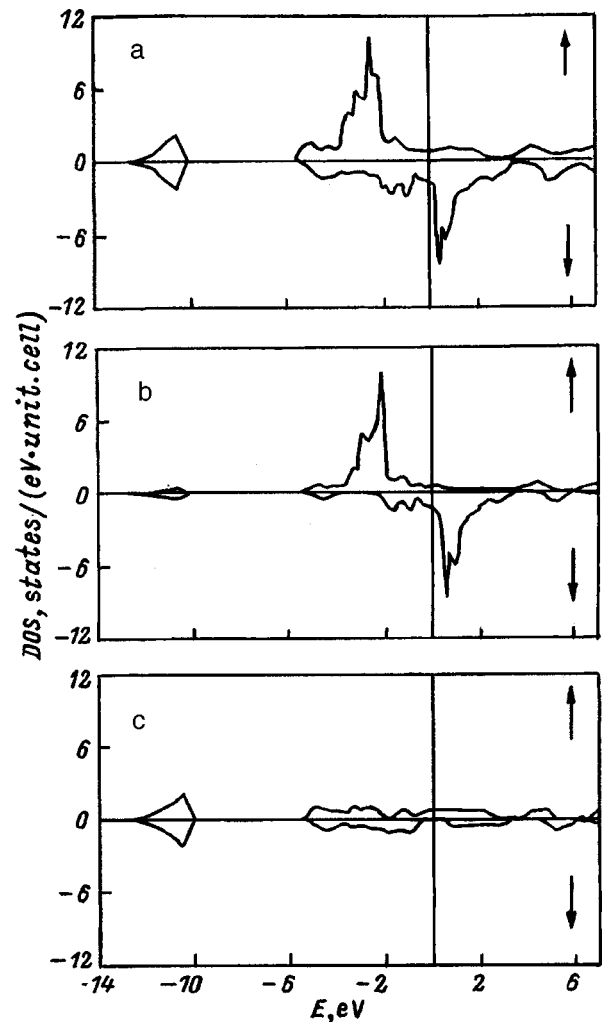
$$\theta_k = \frac{4\pi}{\omega} \operatorname{Re} \left[ \frac{\sigma_{xy}}{(1 - (n + ik)^2)(n + ik)} \right], \quad (1)$$

where  $n + ik$  is the complex refractive index at frequency  $\omega$ . Several microscopic-scale mechanisms can be proposed to account for the large Kerr effect in Mn/Dy/Bi films, which may lead to an increase of  $\sigma_{xy}$  in the presence of a Dy buffer:

1. As already mentioned, the large Kerr effect in MnBi may be due to the 6p–3d electronic transitions (see Fig.

FIG. 3.  $\theta_k$  dispersion relations for (1) Mn/Dy/Bi and (2) MnBi films.

4a–4c), whose matrix elements enter  $\sigma_{xy}$ . Incorporation of Dy atoms in the MnBi lattice may distort the symmetry and give rise to the associated increase in the 6p–3d transition probability, i.e., to an increase of the corresponding matrix elements. The symmetry is distorted when impurity atoms occupy intermediate positions in the MnBi cell.<sup>13</sup> As already pointed out, Dy atoms in Mn/Dy/Bi films have a higher probability to occupy intermediate positions, and this may be one

FIG. 4. MnBi densities of states.<sup>12</sup> (a) joint DOS, (b) density of Mn3d states, (c) density of Bi6p states. The vertical arrows in Figs. 4–6 refer to spin direction.

of the reasons for the enhanced Kerr effect. Our MnBiDy films prepared by codeposition of the components, the conditions favoring substitution of Dy atoms for Mn,<sup>4</sup> exhibit a substantially smaller  $\theta_k$  (Table I).

2. The off-diagonal term of the optical-conductivity tensor can be expanded in terms depending on electron spin orientation<sup>15</sup>

$$\sigma_{xy} = \sigma_{xy}(\uparrow\uparrow) + \sigma_{xy}(\downarrow\downarrow) + \sigma_{xy}(\uparrow\downarrow) + \sigma_{xy}(\downarrow\uparrow). \quad (2)$$

A comparison of the energy dependences of these terms shows that transitions involving spin mixing yield an insignificant contribution, and calculations<sup>13</sup> suggest that the magneto-optical transition in MnBi is dominated by transitions from the  $6p$  spin-down state of Bi to  $3d$ -Mn spin-down states. As seen from Fig. 4b, the Mn $3d$  band is totally polarized, and impurities should not affect it noticeably. An analysis of the electronic structure of MnBiAl films leads to the conclusion that Al doping gives rise to a considerable polarization of the Bi $6p$  band, i.e., to an increase in the number of  $6p$  spin-down electrons and spin-up holes, and that this should enhance the MO effect.<sup>17</sup> Dysprosium in Mn/Dy/Bi films could act in this way. The mechanism underlying this interaction may be hybridization of the Dy $4f$  and  $5d$  states with the Bi $6p$  states (Fig. 4b), which increases the density of states of Bi below the Fermi level, and this, in its turn, should result in an increase of the optical transition probability.

3. The discussion of the Kerr effect in Mn/Dy/Bi films can be facilitated by simulating the electronic structure of this system through superposition of Dy levels on the MnBi band structure. The RE  $s$  and  $d$  electrons in the compound form metallic bonds, whereas the  $4f$  electrons can apparently be considered in a single-impurity approximation as an ensemble of isolated (disregarding hybridization with Mn and Bi) local terms. These terms can shift relative to those of the pure metal. According to XPS data, this shift depends on the percentage content of the RE element,<sup>22</sup> and for Tb<sub>21</sub>Fe<sub>79</sub> amorphous films, for instance, is about 1 eV (Ref. 23). It is believed to be due to  $d$ -state hybridization between Fe and Tb.<sup>23</sup> The spectrum of Tb<sub>21</sub>Fe<sub>79</sub> contains a low-energy maximum with a binding energy of 2–3 eV corresponding to Tb $4f$  electrons. For low binding energies,  $E_b \approx 1 - 3$  eV, the density of states of the RE element is dominated by the  $5d$  electrons (which is also supported by XPS data<sup>24</sup> for pure RE elements), which are responsible for the maximum in the optical conductivity  $\sigma(\omega)$  at  $h\omega \approx 2$  eV.<sup>25</sup> Because RE  $5d \rightarrow$  Mn $3d$  transitions are forbidden by optical selection rules,  $d$  states of an RE element are insignificant from the standpoint of optical transitions.

The  $4f$  electrons in Mn/Dy/Bi films are in the ferromagnetic matrix and can be magnetized by  $s$ - $f$  exchange coupling. In this case, however, in contrast to pure RE elements, where intratomic  $s$ - $f$  exchange interaction is dominant,  $J_{s-f} \sim 1$  eV,<sup>26</sup> the  $4f$  electronic spins interact also with the band electrons of Mn, and this interaction is an order of magnitude weaker. Therefore, one may neglect the exchange splitting of the  $4f$  levels and present the Mn/Dy/Bi band-structure model as a superposition of the Dy density of states in Fig. 4a. Because of the lack of literature data on the den-

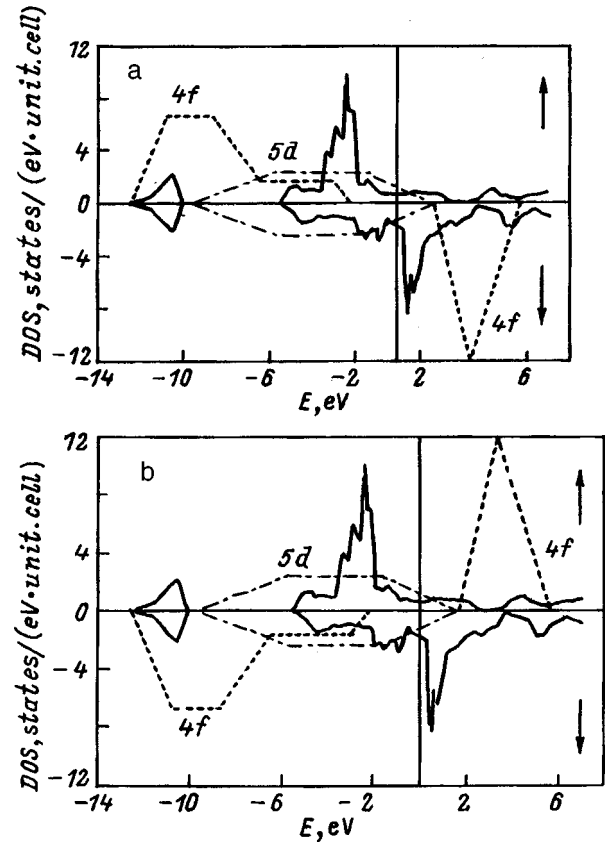


FIG. 5. Superposition of MnBi and Dy DOS for (a) parallel and (b) anti-parallel Mn and Dy spin orientation.

sity of states of Dy in a compound, one can use for this purpose the local density of states of Tb,<sup>27</sup> which was derived<sup>23</sup> directly from XPS and XPS<sup>-1</sup> spectra for Tb<sub>21</sub>Fe<sub>79</sub>. This density of states, calculated taking into account the joint density-of-states function for ferromagnetic Gd,<sup>28</sup> is shown in Fig. 5a by dashed and dot-and-dash lines for the  $4f$  and  $5d$  electrons of Dy at  $T=0$ . The hybridization of the  $4f$  and  $5d$  electrons of Dy with the  $3d$  electrons of Mn was taken into account. The case of parallel Dy and Mn spin orientation, i.e.  $M_{Dy} \uparrow \uparrow M_{Mn}$ , and  $J_{df} > 0$  was considered. It is assumed that there is no spin splitting of the Dy  $5d$  band, or it is very small. Based on this model, Fig. 5a can permit us to find the additional transitions contributing to the Kerr effect enhancement that can be induced by incorporation of Dy. These transitions are listed in Table II. Figures 4 and 5a offer a possibility of making a rough estimate of the contributions due to these transitions. The transitions numbered 1, 4, 5, and 8 should not contribute, because the density of  $6p$  states should already be involved in the transitions observed in MnBi, i.e., Bi $6p$ -Mn $3d$ . The intensity of transition 6 is extremely weak because of the low density of unoccupied spin-up Mn  $3d$  states. The contributions due to the other transitions are of about the same order of magnitude. The above figures permit determining the limits on the energy of each transition, which are also given in Table II. By the transition energy  $\Delta E$  one understands the difference between the energies of the final and initial states. The subscript  $i$  on

TABLE II. Possible transitions in Mn/Dy/Bi films for parallel Dy and Mn spin orientation.

No. n/n	Possible transitions	Transition energy	Significant transition interval, nm
1	$5d \uparrow \rightarrow 6p \uparrow$	$\Delta E > 0$	400–1000
2	$5d \downarrow \rightarrow 6p \downarrow$	$\Delta E > 0$	400–1000
3	$6p \uparrow \rightarrow 5d \uparrow$	$0 < \Delta E < E_{5d\uparrow}$	770–1000
4	$6p \downarrow \rightarrow 5d \downarrow$	$0 < \Delta E < E_{5d\downarrow}$	770–1000
5	$4f \uparrow \rightarrow 6p \uparrow$	$\Delta E > E_{f\uparrow}$	400–860
6	$4f \uparrow \rightarrow 3d \uparrow$	$\Delta > E_{f\uparrow}$	400–860
7	$4f \uparrow \rightarrow 5d \uparrow$	$E_{f\uparrow} + E_{5d\uparrow} > \Delta E > E_{f\uparrow}$	400–860
8	$6p \downarrow \rightarrow 4f \downarrow$	$E_{f\downarrow} + \Delta E_{f\downarrow} > \Delta E > E_{f\downarrow}$	400–860
9	$3d \downarrow \rightarrow 4f \downarrow$	$E_{f\downarrow} + \Delta E_{f\downarrow} > \Delta E > E_{f\downarrow}$	400–860
10	$5d \downarrow \rightarrow 4f \downarrow$	$E_{f\downarrow} + \Delta E_{f\downarrow} > \Delta E > E_{f\downarrow}$	400–860

the energy identifies the edge of the density-of-*i*-states band closest to the Fermi level.

Table III presents similar data for the case of antiparallel Dy and Mn spin orientation. The corresponding density-of-states function is shown in Fig. 5b. One readily sees that the transitions labeled 1 and 4 do not contribute for the above-mentioned reason. The intensities of transitions 2, 3, 5, 7, 8, and 9 are of about the same order of magnitude, because the densities of the corresponding initial and final states differ insignificantly. Transition 10 may provide a noticeable contribution. Note also the  $4f \downarrow \rightarrow 3d \downarrow$  transition, which may become strong under certain conditions.

The limits on the energies of possible transitions can be estimated quantitatively taking due account of the fact that the edges of the Dy4*f* bands may differ from those presented in Fig. 5a and 5b for Tb. Published XPS data suggest that the maximum in the density of Dy4*f* states in RE-Fe<sub>2</sub> lies closer to the Fermi level than that for Tb.<sup>29</sup> Tables II and III give the ranges for the contribution of possible transitions, which were determined under the assumption that the filled 4*f* band is shifted toward the Fermi level only by 1 eV compared to the diagram in Figs. 4 and 5a, i.e.,  $E_{f\downarrow} = -1.4$  eV, and the others, in accordance with the figure, are  $E_{3d\downarrow} = 0.3$  eV,  $\Delta E_{3d\downarrow} = 0.5$  eV,  $E_{f\uparrow} = 2.6$  eV, and  $\Delta E_{f\uparrow} = 3$  eV. Note also that this shift should be accompanied by about the same shift of the unfilled 4*f* band toward higher energies,<sup>27</sup> and vanish-

TABLE III. Possible transitions in Mn/Dy/Bi films for antiparallel Dy and Mn spin orientation.

No. n/n	Possible transitions	Transition energy	Significant transition interval, nm
1	$5d \uparrow \rightarrow 6p \uparrow$	$\Delta E > 0$	400–1000
2	$5d \downarrow \rightarrow 6p \downarrow$	$\Delta E > 0$	400–1000
3	$6p \uparrow \rightarrow 5d \uparrow$	$0 < \Delta E < E_{5d\uparrow}$	770–1000
4	$6p \downarrow \rightarrow 5d \downarrow$	$0 < \Delta E < E_{5d\downarrow}$	770–1000
5	$4f \downarrow \rightarrow 6p \downarrow$	$\Delta E > E_{f\downarrow}$	400–860
6	$4f \downarrow \rightarrow 3d \downarrow$	$E_{f\downarrow} + E_{3d\downarrow} + \Delta E_{3d\downarrow} > \Delta E > E_{f\downarrow} + E_{3d\downarrow}$	560–730
7	$4f \downarrow \rightarrow 5d \downarrow$	$E_{f\downarrow} + E_{5d\downarrow} > \Delta E > E_{f\downarrow}$	400–860
8	$6p \uparrow \rightarrow 4f \uparrow$	$E_{f\uparrow} + \Delta E_{f\uparrow} > \Delta E > E_{f\uparrow}$	400–500
9	$3d \uparrow \rightarrow 4f \uparrow$	$E_{f\uparrow} + \Delta E_{f\uparrow} > \Delta E > E_{f\uparrow}$	400–500
10	$5d \uparrow \rightarrow 4f \uparrow$	$E_{f\uparrow} + \Delta E_{f\uparrow} > \Delta E > E_{f\uparrow}$	400–500

ing of the contributions due to transitions terminating on unfilled 4*f* states.

As seen from Table II, in the case of  $M_{Dy\uparrow} \uparrow M_{Mn}$  the contributions due to possible transitions should be uniformly distributed within the 400–1000-nm wavelength range under consideration. The intensities of these transitions are of about the same order of magnitude, i.e., they can produce only a shift of the spectral curve as a whole toward higher values of  $\theta_k$  and cannot give rise to the energy shift of the maximum observed for Mn/Dy/Bi, which, as in the case of MnBi, is provided by the  $Bi6p \downarrow \rightarrow Mn3d \downarrow$  transitions. The pattern for the  $M_{Dy\downarrow} \uparrow M_{Mn}$  case is approximately the same. The relevant transition  $4f \downarrow \rightarrow 3d \downarrow$ , however, should contribute substantially within the wavelength interval determined by the width of the peak of unfilled  $Mn3d \downarrow$  states, and it corresponds in this case to the interval of the observed maximum in the Kerr effect. There are unfortunately no data on the mutual orientation of the Dy and Mn spins, and the decrease in magnetization observed in Mn/Dy/Bi films cannot be considered as evidence for their antiparallel orientation, because it can be caused by a decrease in crystallite size.<sup>17</sup>

In Mn compounds with Dy one observes both ferromagnetic<sup>30</sup> and antiferromagnetic<sup>31</sup> spin ordering of these elements, with the magnetic properties depending to a considerable extent on interatomic distance<sup>32</sup>. It may be conjectured that ordering, similar to RE(Fe,Co)<sup>33</sup> compounds, varies from antiferromagnetic to ferromagnetic with increasing distance between the RE and Mn atoms. If Dy atoms occupy intermediate positions in the MnBi cell, the distance between the Mn and Dy atoms is larger than when they substitute for Bi atoms, i.e. in the second case antiferromagnetic ordering is more probable. As already mentioned, the Dy positions depend on the technology by which the Dy was incorporated, and, hence, the differences in the MO properties between Mn/Dy/Bi and MnBiDy films may be due to the fact that these films differ to a certain extent in the mutual ordering of Mn and Dy spins and in the corresponding contributions due to the above transitions.

For the case  $M_{Dy\uparrow} \uparrow M_{Mn}$ , if the unfilled 4*f* band is narrow enough, the maximum in the Kerr effect can be assigned to transitions to this band. The interval within which these transitions provide a contribution should be determined by the width of the peak of unfilled 4*f* states, so that, for instance, in the case of  $E_{f\downarrow} = 1.6$  eV corresponding to Fig. 6a and  $\Delta E_{f\downarrow} \sim 0.8$  eV it extends from 520 to 770 nm. Hence such transitions may produce the maximum in  $\theta_k$  observed exactly within this wavelength interval. Electronic structure calculations, which were carried out by means of the LMTO method localized to a maximum extent and were based on the atomic-sphere approximation and the recursive approach, showed that the position and width of the peak of unfilled 4*f* states in RE-TM amorphous films depend on the RE type.<sup>34</sup> It was shown also that variation of interatomic distance within 1 to 2% for the same atomic content shifts this peak by 0.3 eV. Hence there is a possibility of varying the width and position of the peak of unfilled 4*f* states by properly choosing the corresponding composition.

Figure 6a and 6b displays the densities of states calculated taking into account the spin splitting of the 5*d* band for

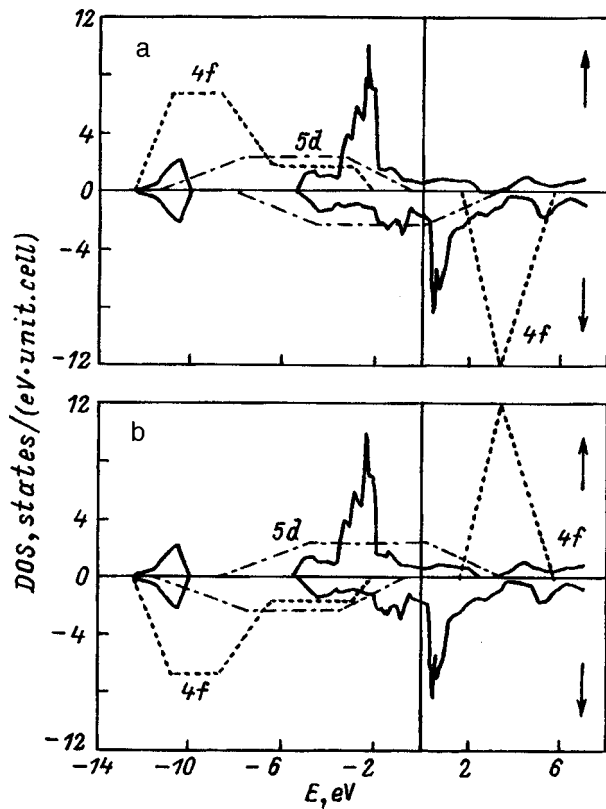


FIG. 6. Superposition of MnBi and Dy DOS with inclusion of the spin splitting of Dy5d band for (a) parallel and (b) antiparallel Mn and Dy spin orientation.

the  $J_{\text{MnDy}} > 0$  and  $J_{\text{MnDy}} < 0$  cases, respectively. Although splittings above 4 eV are not likely,<sup>35</sup> it is this limiting case that is depicted in the figure. An estimate of the intensity of the additional transitions shows that in the  $M_{\text{Dy}}\uparrow\uparrow M_{\text{Mn}}$  case the transitions terminating on the  $5d\uparrow$  state (transitions 3 and 7 in Table II) are no longer operative, as are also transitions 4 and 7 in Table III ending on the  $5d\downarrow$  state in the  $M_{\text{Dy}}\downarrow\uparrow M_{\text{Mn}}$  case. Because these transitions cover together the whole wavelength interval considered here, it can be assumed that the spectral curve undergoes a lowering as a whole in both cases, although there is a certain increase in intensity for transitions starting from the  $5d\downarrow$  state (transition 10) in the first case and from the  $5d\uparrow$  state in the second (transition 10). All the other transitions do not change.

A more detailed consideration made for the  $M_{\text{Dy}}\uparrow\uparrow M_{\text{Mn}}$  case (Fig. 6a) shows that the effect of splitting depends on temperature. As the temperature increases, the  $5d\uparrow$  band shifts toward the Fermi level and crosses it at a temperature  $T = T^*$ . For  $T > T^*$ , the transitions which disappeared because of the splitting,  $\text{Bi}6p\uparrow \rightarrow \text{Dy}5d\uparrow$  and  $\text{Dy}4f\uparrow \rightarrow \text{Dy}5d\uparrow$ , become operative again, to be accompanied by a growth in conductivity. A similar situation is observed in the  $M_{\text{Dy}}\downarrow\uparrow M_{\text{Mn}}$  case (Fig. 6b), i.e., at  $T = T^*$  the vanished transitions,  $6p\downarrow \rightarrow 5d\downarrow$  and  $4f\downarrow \rightarrow 5d\downarrow$ , reappear, to give rise to an upward shift of the  $\theta_k$  spectral response as a whole.

Thus the model proposed here permits a detailed analysis of the contribution to the MO effect due to additional transitions which may be induced by Dy doping. One may

thus conclude that, if the filled Dy4f band in Mn/Dy/Bi films lies sufficiently close to the Fermi level, a maximum in the  $\theta_k$  spectrum may appear only for antiparallel orientation of Dy and Mn spins, and it will be dominated by  $4f\downarrow \rightarrow 3d\downarrow$  transitions. If the unfilled 4f band is very narrow and is located sufficiently close to the Fermi level, then a maximum may appear in the spectrum due to new transitions only in the parallel-orientation case. This maximum may be contributed by  $6p\downarrow \rightarrow 4f\downarrow$ ,  $3d\downarrow \rightarrow 4f\downarrow$ , and  $5d\downarrow \rightarrow 4f\downarrow$  transitions. As already pointed out, the shift of the unfilled 4f band toward the Fermi level should be accompanied by the corresponding shift of the edge of the filled 4f band toward higher binding energies,<sup>27</sup> and it is this band (i.e. the  $4f\downarrow \rightarrow 3d\downarrow$  transitions) that will account for the maximum in the Kerr effect observed<sup>13</sup> in the short-wavelength region. The spin splitting of the 5d band lowers the  $\theta_k$  spectral-response curve, which rises again with increasing temperature.

The present consideration of the reasons which may be responsible for the Kerr effect enhancement in Mn/Dy/Bi films is of a preliminary nature. Further structural studies of such films, as well as theoretical calculations taking into account different positions of Dy atoms in the MnBi cell, investigation of the optical and magneto-optic properties made within a broader wavelength range and for different temperatures, combined with XPS analysis, will offer a possibility of corroborating the influence of the above factors on the Kerr effect, as well as to determine quantitatively the contribution of each of them to its enhancement.

<sup>1</sup> H. J. Williams, R. C. Sherwood, F. G. Foster, and E. M. Kelley, J. Appl. Phys. **28**, 1181 (1957).

<sup>2</sup> K. Egashira and T. Yamada, J. Appl. Phys. **45**, 3643 (1974).

<sup>3</sup> L. V. Burkova, A. S. Parshin, V. A. Serezhkin, and V. Yu. Yakovchuk, Avtometriya No. 2, 39 (1995).

<sup>4</sup> W. K. Unger, E. Wolfgang, H. Harms, and H. Haudek, J. Appl. Phys. **43**, 2875 (1972).

<sup>5</sup> H. Göbel, E. Wolfgang, and H. Harms, Phys. Status Solidi A **35**, 89 (1976).

<sup>6</sup> Y. J. Wang, J. X. Shen, and Q. Tang, J. Magn. Magn. Mater. **74**, 365 (1988).

<sup>7</sup> A. Katsui, A. Shibukawa, H. Terui, and K. Egashira, J. Appl. Phys. **47**, 5069 (1976).

<sup>8</sup> Y. Chen, C. P. Luo, Z. T. Guan, Q. Y. Lu, and Y. J. Wang, J. Magn. Magn. Mater. **115**, 55 (1992).

<sup>9</sup> A. Katsui, J. Appl. Phys. **47**, 4663 (1976).

<sup>10</sup> Y. J. Wang, J. Magn. Magn. Mater. **84**, 39 (1990).

<sup>11</sup> D. S. Dai, R. Y. Fang, P. Long, S. Zhang, T. J. Ma, C. Dai, and X. X. Zhang, J. Magn. Magn. Mater. **115**, 66 (1992).

<sup>12</sup> R. Coehoorn and R. A. de Groot, J. Phys. F **15**, 2135 (1985).

<sup>13</sup> J. Köhler and J. Kübler, J. Phys.: Condens. Matter **8**, 8681 (1996).

<sup>14</sup> P. M. Oppeneer, V. N. Antonov, T. Kraft, H. Eschrig, A. N. Yaresko, and A. Ya. Perlov, J. Appl. Phys. **80**, 1099 (1996).

<sup>15</sup> D. K. Misemer, J. Magn. Magn. Mater. **72**, 267 (1988).

<sup>16</sup> K. W. Wierman, J. X. Shen, R. D. Kirby, and D. J. Sellmyer, J. Appl. Phys. **75**, 6348 (1994).

<sup>17</sup> Z. Li, H. Luo, W. Lai, Z. Zeng, and Q. Zheng, J. Magn. Magn. Mater. **98**, 47 (1991).

<sup>18</sup> V. A. Serezhkin, V. Yu. Yakovchuk, L. V. Burkova, and S. Z. Sklyuev, USSR Inventor's Certificate No. 1718273 (1992).

<sup>19</sup> M. Masuda, I. Izawa, S. Yoshino, S. Shiomi, and S. Uchiyama, Jpn. J. Appl. Phys. **26**, 707 (1987).

<sup>20</sup> D. Chen, J. Appl. Phys. **42**, 3625 (1971).

<sup>21</sup> R. B. van Dover, E. M. Gyorgy, R. P. Frankenthal, M. Hong, and D. J. Siconolfi, J. Appl. Phys. **59**, 1291 (1986).

<sup>22</sup> A. S. Andreenko and L. Zhanda, Fiz. Tverd. Tela (Leningrad) **30**, 1530 (1988) [Sov. Phys. Solid State **30**, 885 (1988)].

- <sup>23</sup>G. A. N. Connell, S. J. Oh, J. Allen, and R. Allen, *J. Non-Cryst. Solids* **61-62**, 1061 (1984).
- <sup>24</sup>P. O. Hedén, H. Löfgren, and S. B. M. Hagström, *Phys. Rev. Lett.* **26**, 432 (1971).
- <sup>25</sup>N. Ahmed-Mokhtar, J. P. Petrakian, R. Philip, R. Fraisse, and B. Lazarides, *Thin Solid Films* **88**, 177 (1982).
- <sup>26</sup>R. Ahuja, S. Auluck, B. Lohansson, and M. S. S. Brooks, *Phys. Rev. B* **50**, 5147 (1994).
- <sup>27</sup>G. A. N. Connell, *J. Magn. Magn. Mater.* **54-57**, 1561 (1986).
- <sup>28</sup>J. Sticht and J. Kübler, *Solid State Commun.* **53**, 529 (1985).
- <sup>29</sup>V. V. Nemoskalenko, V. N. Uvarov, S. V. Borisenko, A. I. Senkevich, and V. D. Borisenko, *Metallofiz. Nov. Tekhnol.* **17**, No. 10, 3 (1995).
- <sup>30</sup>S. Labroo, N. Ali, and P. Robinson, *J. Appl. Phys.* **67**, 5292 (1990).
- <sup>31</sup>K. Yoshimura, M. Shiga, and Y. Nakamura, *J. Phys. Soc. Jpn.* **55**, 3585 (1986).
- <sup>32</sup>H. Wada, H. Nakamura, K. Yoshimura, M. Shiga, and Y. Nakamura, *J. Magn. Magn. Mater.* **70**, 134 (1987).
- <sup>33</sup>K. N. R. Taylor and M. I. Darby, *Physics of Rare-Earth Solids* [Chapman and Hall, London, 1972; Mir, Moscow, 1974], 374 pp.
- <sup>34</sup>H. Tanaka and S. Takayama, *J. Appl. Phys.* **67**, 5334 (1990).
- <sup>35</sup>Yu. V. Knyazev and G. A. Bolotin, *Fiz. Met. Metalloved.* **58**, 1121 (1984).

Translated by G. Skrebtsov